Soft Matter

Accepted Manuscript

This article can be cited before page numbers have been issued, to do this please use: V. Vitali, G. Nava, A. Corno, M. Pezzotti, F. Bragheri, P. Paiè, R. Osellame, M. A. Ortenzi, I. Cristiani, P. Minzioni, T. Bellini and G. Zanchetta, *Soft Matter*, 2021, DOI: 10.1039/D0SM02168G.

ROYAL SOCIETY OF CHEMISTRY

rsc.li/soft-matter-journal

View Article Online
DOI: 10.1039/D0SM02168G

Soft Matter

ARTICLE TYPE

Cite this: DOI: 00.0000/xxxxxxxxxx

Yield stress "in a flash": investigation of nonlinearity and yielding in soft materials with an optofluidic microrheometer†

Valerio Vitali,[a*] Giovanni Nava,[b] Andrea Corno,[b] Melissa Pezzotti,[a] Francesca Bragheri,[c] Petra Paiè,[c] Roberto Osellame,[c,d] Marco Aldo Ortenzi,[e] Ilaria Cristiani,[a] Paolo Minzioni,[a] Tommaso Bellini,[b] and Giuliano Zanchetta[b**]

Received Date
Accepted Date

DOI: 00.0000/xxxxxxxxxx

Yield stress materials deform as elastic solids or flow as viscous liquids, depending on the applied stress, which also allows them to trap particles below a certain size or density threshold. To investigate the conditions for such a transition at the microscale, we exploit an optofluidic microrheometer, based on the scattering of an infrared beam onto a microbead, which reaches forces in the nN scale. We perform creep experiments on a model soft material composed of swollen microgels, determining the limits of linear response and yield stress values, and we find quantitative agreement with bulk measurements. However, the motion of the microbead, both below and above yielding, reflects distinctive microscale features of the surrounding material, whose plastic rearrangements we investigate through small, passive tracers.

1 Introduction

The relevance of soft materials for our daily life is strongly nested in their multiple length scales and rich mechanical behaviour, viscoelastic response and flow properties. In particular, yield stress materials (found e.g. in food, biological networks, cosmetics) deform as elastic solids or flow as viscous liquids, depending on whether the stress applied upon them is below or above a threshold stress called yield stress, σ_y [1–4] . The origin and conditions of such a transition display several open issues, like the stress distribution within the material or the role of microstructural dynamics in determining slow creep rearrangements before yielding[2].

The possibility to switch from a solid to a fluid behaviour is also at the basis of the widespread application of yield stress fluids in personal care products[5,6], in particular for their ability to suspend and trap density-mismatched particles, either lighter or heavier than the matrix, which would otherwise cream or sediment[7,8]. The threshold condition for stable trapping in a yield stress fluid[9] can be expressed in terms of the ratio between the bulk σ_y and the total gravitational stress of the particle[1,10]:

$$Y = \frac{\sigma_y 2\pi R^2}{\frac{4}{3}\pi R^3(\rho_p - \rho_s)g} = \frac{1.5\sigma_y}{R(\rho_p - \rho_s)g} \quad (1)$$

where R is the particle radius and ρ_p and ρ_s are particle and solvent density, respectively. In general, the stress exerted by a particle scales as a force over a surface, or an effective cross-section; specifically, in Eq. 1 half of the particle surface is considered. The problem has been extensively investigated, mostly for millimeter- to centimeter-sized particles, both experimentally[11–13] and numerically[10,14]. The Y value is typically found to be between 0.14 and 0.2. In general, this implies that the gravitational stress is distributed onto a portion of material 1/Y times larger than the geometric cross section of the particle itself. Equivalently, the particle can only flow through the yield stress material if a region of material 1/Y times the geometric cross section is displaced, or fluidized. However, the specific threshold value can sensitively depend on the material's microstructure[7] and the validity of this approach down to the microscale has not been investigated. In general, the connection between bulk rheological properties and local behaviour around a particle is not trivial, as it can depend on the relevant length scales of the system.

Local yielding mechanisms can be directly elucidated by probing rheological properties at the microscale and comparing them to

[a]Dipartimento di Ingegneria Industriale e dell'Informazione, Università di Pavia, 27100 Pavia, Italy
[b]Dipartimento di Biotecnologie Mediche e Medicina Traslazionale, Università di Milano, 20090 Segrate (MI), Italy. E-mail: giuliano.zanchetta@unimi.it
[c]Istituto di Fotonica e Nanotecnologie (IFN), Consiglio Nazionale delle Ricerche (CNR), 20133 Milano, Italy
[d]Dipartimento di Fisica, Politecnico di Milano, 20133 Milano, Italy
[e]CRC Materiali Polimerici (LaMPo), Dipartimento di Chimica, Università di Milano, 20133 Milano, Italy
*Currently at Optoelectronics Research Centre, University of Southampton, Southampton, Hampshire, SO17 1BJ, UK

† Electronic Supplementary Information (ESI) available: [details of any supplementary information available should be included here]. See DOI: 10.1039/cXsm00000x/

View Article Online
DOI: 10.1039/D0SM02168G

bulk behaviour. To this aim, active microrheology techniques[15,16] are best suited, as they consist in the application of an external - optical or magnetic - force to a microbead and in the observation of its resulting motion, which is the local counterpart of the creep tests typically performed in bulk rheometry to estimate yield stress. Magnetic tweezers can exert high (but inhomogeneous) forces above 1 nN[17] and have been used to characterize yield stress properties of an aging clay[18], but the inertia of the bulky setup required for this technique makes it non-ideal for high-frequency or time-resolved experiments. On the contrary, optical tweezers, based on trapping and manipulation of a microparticle in the waist of a laser beam through gradient optical forces[19], offer tremendous versatility and speed; indeed, they are widely used to characterize the microrheology of a variety of viscoelastic materials, from colloidal suspensions to biopolymer networks[20,21]. However, the maximum attainable force is below 100 pN[15], which limits their use for yield stress investigation. Furthermore, optical tweezers can typically trap particles of up to a couple of μm, which can be a strong limitation in terms of accessible material length scales[22].

Here, we apply an alternative optical, active microrheology technique, based on the scattering force exerted by an incident beam on a microbead[23], which can push the particle along the optical axis. Although it is not easy to fully compare the magnitude of gradient and scattering force, as they strongly depend on beam and bead parameters, using the scattering force, instead of the gradient one, yields several advantages. First of all, the scattering force is less sensitive to particle diameter and particle position. Additionally, the scattering force grows monotonically by increasing the bead refractive index, while gradient force has a more complex behaviour and can even be reversed in case of very high (e.g. >5) refractive index particles. Furthermore, by combining a microfluidic chip with waveguides fabricated in glass via femtosecond laser micromachining[24–26], an excellent spatial and temporal control can be obtained over force application. Indeed, the device has been recently applied for the microrheological characterization of viscoelastic surfactant solutions[27] and DNA hydrogels[28]. We demonstrate here a simple but effective implementation of our setup to perform the first optical microrheology creep experiments, thanks to the fine control over the applied force and its amplitude up to 1 nN. With this approach, we characterize the yielding of an aqueous suspension of packed, swollen microgels, a well studied example of simple yield stress fluid[12,29]. From the different regimes observed in the motion of the microbead at different applied forces, linear and yielding properties of the material are readily estimated. We find good agreement with bulk rheology measurements. However, the details of microbead trajectory, and its effects on the surrounding material, offer some hints on the microscopic mechanism of yielding. The microbead, both at low and high forces, advances in a series of small yielding events corresponding to intermittent or periodic microgel rearrangements within the material. Furthermore, small passive tracers allow us to estimate the extent of the fluidized region around the microbead, which agrees with previous estimates for large particles.

2 Materials and methods

2.1 Materials

Carbopol Aqua SF2 (Lubrizol) batch solution was diluted to the desired concentration at acidic pH, which guarantees a fully fluid, yet turbid, sample. pH was then slowly increased by addition of drops of NaOH 10 M while stirring, until around pH 7 the microgels swelled, the sample became transparent and developed a yield stress. The sample was gently mixed for 24 hours and displayed stable behaviour for several weeks.

As probe particles, we used either polystyrene (PS) microbeads with diameter 10 μm and refractive index 1.57 at 1070 nm (Sigma Aldrich 72986), or glass microbeads with a large percentage of Titanium Oxide and Barium Oxide (TBG), with refractive index 1.9 at 589 nm (Cospheric BTGMS-4.15 5-22um). We determined the refractive index of TBG microbeads at the wavelength of 1070 nm used in the microrheology experiments to be equal to 1.85 ± 0.03 (see Supplementary Information). Because of the higher index, TBG microbeads allow achieving a maximum value of the optical force almost 3 times larger than PS microbeads, at the same power level and for the same probe dimension (see Supplementary Information). Particles with diameter around 10 μm were selected from the polydispersed batch and their size carefully measured. Fluorescent polystyrene tracers (Microparticles GmbH PS-FluoRed-0.5, mean diameter 0.45 μm) were dispersed in the Aqua samples for strain field determination.

2.2 Macroscopic rheology

Macroscopic rheological tests were performed on a Physica MCR 302 rheometer (Anton Paar GmbH) using a cone and plate geometry with a cone radius of 25 mm and a cone angle of 1°. The temperature was controlled to 23 °C by a Peltier element and evaporation was minimized by surrounding the sample with fluorinated oil. A fresh sample was loaded for each series of experiments and reproducibility was checked by repeating some tests several times. Creep and recovery experiments were performed by applying and subsequently removing step stresses, with time intervals identical to the microrheology experiments. Flow curve tests were performed by applying a steady strain rate, decreasing from 100 to 10^{-2} s^{-1} in 40 steps, using logarithmically increasing sampling times to ensure steady state conditions at all shear rates.

2.3 Active microrheology

2.3.1 Experimental setup

A sketch of the experimental setup used for active microrheology experiments is shown in Fig. 1. A CW Yb-doped fiber laser (YLD-10-1064, IPG Photonics, Pmax = 10 W at 1070 nm) is used as optical source and connected to a fiber-to-fiber U-bench, so as to have a direct and easy access to the laser beam. A shutter, whose movement is controlled by a motorized stage, is located inside the U-bench, thus allowing to block/unblock the laser radiation. The output of the U-bench is then connected to an optical waveguide in the optofluidic chip, which represents the core element of the microrheological setup. This integrated system is

View Article Online
DOI: 10.1039/D0SM02168G

realised by femtosecond-laser writing of optical waveguides in a commercial microfluidic chip (Translume Inc., Ann Arbor, MI, USA), which is also fabricated through femtosecond-laser micromachining and chemical etching in a fused silica substrate. The micro-opto-fluidic chip comprises a straight microfluidic channel with a square cross section of 150 $\mu m \times 150\ \mu m$ and a pair of facing waveguides inscribed at half of the channel height (75 μm from the bottom) on the two sides of the channel. The optical radiation emitted by the two waveguides can be used to manipulate the position of microbeads dispersed in the microchannel and hence, by tracking their movement, to infer the rheological properties of the surrounding fluid, as previously reported in[26–28]. Here, to exert a constant force and perform creep experiments a single waveguide is needed. The chip is mounted on the plate of a phase-contrast inverted microscope and the microbead movement is monitored by a CMOS camera (DCC1545M Thorlabs, maximum 250 frames per second) connected to the microscope. Finally, the pressure and hence the sample flow inside the microchannel can be precisely controlled by a micropump, whose tubing is screwed to one of the two Luer connectors glued on the top surface of the chip. All the instruments are remotely controlled by a computer through a custom-made Labview script.

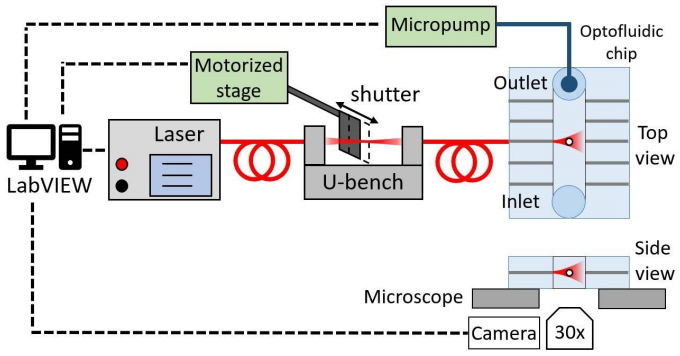

Fig. 1 Schematic diagram of the microrheology experimental setup. The dashed black lines represent the electrical cables connections while the thick red lines represent the optical fibers connections.

2.3.2 Measurement protocol

The sample to be characterized is prepared by dispersing a small amount of tracers (PS or TBG microbeads) into the material under test and is then injected into the microfluidic chip reservoir using a standard micro-pipette. The gravitational stress acting on the microbead is typically well below the yield stress of the material, so that, when the laser is off, the microbeads are stably trapped at different heights in the microchannel, with no detectable motion. By flowing the sample, a suitable bead is selected in the midplane of the microchannel, so to match the height of the waveguide. The laser source is set at the desired optical power, with the shutter initially closed. The microbead inital position is recorded for few seconds, then the shutter is opened (the opening time is few ms) and, as a result, the microbead is optically pushed due to the scattering force exerted by the laser beam ("optical shooting" technique[26]). After a preset time, the optical force is switched off by closing the shutter and the microbead recovery is monitored for a fixed time. This procedure is repeated for different values of the optical power emitted by the laser source and several microbeads dispersed in different positions along the channel, limiting the duration of the experiments and refreshing the sample also to avoid artifacts related to heating[27] and degradation.

2.3.3 Microrheometer calibration

We calibrated the optical force inside the channel by tracking the displacement of PS microbeads in Newtonian fluids of known viscosity η. In this case, the applied optical force F_o equals the Stokes drag force $F_s = 6\pi R\eta v$ and the resulting microbead velocity is given by $v = F_o/(6\pi R\eta)$, due to the combined effect of shear and compression of the surrounding fluid[1]. As a consequence, by defining the average strain γ as the ratio between microbead displacement (Δx) and its diameter, $\gamma = \Delta x/(2R)$, the stress acting on the microbead $\sigma = \eta\dot{\gamma}$ is naturally defined as

$$\sigma = \frac{F_o}{12\pi R^2}. \tag{2}$$

We thus adopted such a definition also in the case of the non-Newtonian fluids studied here, as generally done in active microrheology[15], although the full strain field and perturbed microstructure should be considered explicitly to properly determine the Stokes component[22].

The optical force acting on the microbead can be written as $F_o = AP_L f(x)$, where A is a calibration constant, P_L is the power emitted by the laser source, which is known, and $f(x)$ is the optical force profile, which can be precisely calculated by means of numerical simulations based on the paraxial ray-optics (PRO) approach[30,31]. The calibration constant A can be determined by performing optical shooting experiments in Newtonian fluids of known viscosity[28], for different values of the laser power (see Supplementary Information). Once the calibration constant is determined, the optical force F_o can be calculated for different laser power levels P_L and different types or sizes of microbeads, by recalculating the proper force profile $f(x)$ to take into account the different microbead properties. Although the force can easily reach hundreds of pN (Fig. 3), the resulting stress is relatively limited, in the Pa scale, because of the rather large size of the microbead ($R = 5\mu m$). However, this guarantees a quasi-continuum probing of the mechanical properties of our microgel sample[22,32]. For materials with smaller typical length scales, smaller microbeads could be safely used, which would increase the accessible stress by at least one order of magnitude. The accessible effective strains, determined by the spatial resolution of microbead tracking (~ 10 nm) and the width of the channel, are between 0.1 and 1000 %. The range of shear rates is also affected on the lower bound by the duration of the experiments, kept at 10 seconds to avoid artifacts from drift or possible heating effects, and on the upper bound by camera acquisition speed, 250 frames per second. These factors, together with the shutter speed, yield shear rates between 10^{-4} and $10^{1}\ s^{-1}$.

View Article Online
DOI: 10.1039/D0SM02168G

3 Results and discussion

3.1 Bulk rheology of microgel suspensions

Like other swollen microgel systems and in particular like other samples of its Carbopol family, Aqua displays fluid-like, weakly viscoelastic behaviour up to a threshold concentration around c = 0.2 % at pH 7, above which a measurable yield stress appears. For various concentrations in the yield-stress region, we performed a creep test on the material with a macroscopic rheometer, by applying a constant shear stress and monitoring over time the resulting strain deformation, as shown in Fig. 2b for c = 0.375%, with color coding for the applied stress. Furthermore, the evolution of strain was followed after removal of the load (Fig. 2a), to estimate the amount of stored and lost deformations.

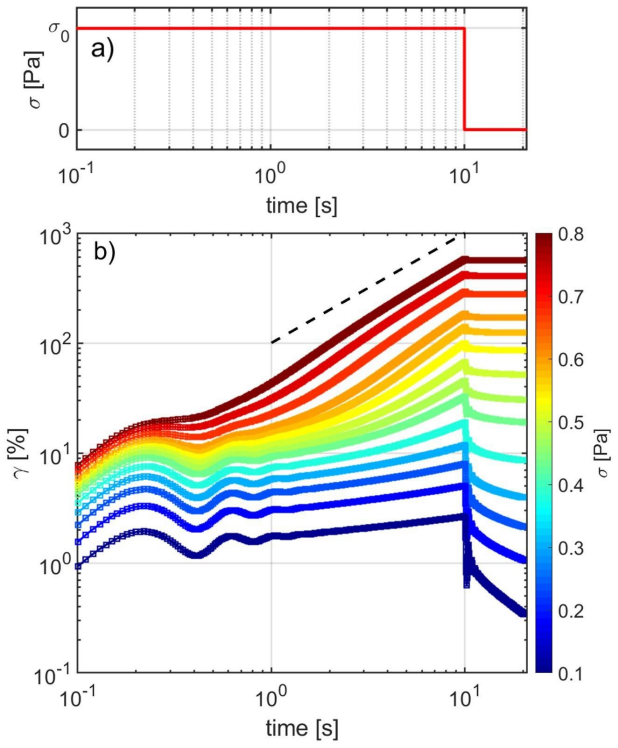

Fig. 2 a) Creep and recovery measurement protocol: a constant stress σ_0 is applied to the sample under test and, after a preset time, the stress is switched off and the material recovery is recorded for a fixed time; b) Results of the macroscopic creep and recovery measurements performed on an Aqua sample at a concentration c = 0.375% by imposing different shear stress values, as indicated by the color bar. The dashed black line represents linear, fluid-like behaviour.

After some oscillations during the first tenths of second, determined by the inertia of the tool, for low applied stresses the strain tends to a fixed value, the expected behaviour for a so-called Kelvin-Voigt solid: an elastic network, whose elastic modulus determines the amplitude of deformation, embedded in a viscous fluid, whose viscosity sets the time scale of the response. Correspondingly, the sample completely recovers its initial state after stress removal. For increasing stresses, a creep regime sets in, with low, sublinear temporal evolution of the strain $\gamma \sim t^{\alpha}$ ($\alpha \ll 1$). Above a certain stress threshold, which we can identify as the yield stress, the material is fluidized and the strain evolution becomes linear, $\gamma \sim t$, as evidenced by the dashed line with slope 1 in Fig. 2b. As the sample is plastically deformed, the recovered strain upon stress removal progressively decreases, approaching a fluid behaviour; however, even at high stresses, a small recoil can be observed, as the material keeps storing some elastic energy for moderate fluid flows.

3.2 Microrheology experiments

We can perform analogous experiments with our microrheology setup, by monitoring the transient microbead displacement upon switching on and off the scattering force in a step-wise fashion. We show such experiments, for various values of the optical force, for the same sample at c = 0.375% in Fig. 3 (in logarithmic and linear scale in panels a and b, respectively). Despite some detectable intermittance or periodicity in the trajectories, which we will discuss below, the overall microrheology behaviour is qualitatively similar to its macroscopic counterpart. The response is mainly elastic and fully reversible for small applied stresses, while for increasing stresses creep motion sets in and only partial recovery is observed; eventually, for high enough stresses, the microbead advances linearly in time (dashed black line in panel a), although with discrete jumps, analyzed in section 3.2.2. A significant recoverable strain persists when the stress is switched off even in the flowing regime.

From the initial response in the creep tests we can obtain an estimate of the short-time elastic component of the material as $G' = \sigma/\gamma(t_{el})$ (see Fig. 4a). We selected $t_{el} = t_{ON} + 0.5$ s, as a time long enough to reach a plateau and at which most of the oscillations were damped in macroscopic experiments, but short enough before the onset of significant creep, so that values could be compared. In Fig. 4b we plot G' as a function of the resulting strain. In macroscopic and microscopic creep measurements (empty squares and color-coded diamonds, respectively) we find two similar trends with a linear regime (G' independent from γ and identical to linear elasticity estimates), followed by a plastic regime. For low stresses, we could also extract the frequency-dependent linear viscoelastic moduli from our microscopic creep data through $i-Rheo$, a method based on Fourier analysis[33,34]. We found weak frequency dependence, in agreement with bulk oscillatory measurements (see Supplementary Fig. S2). To properly estimate the σ_y values from creep and recovery experiments, we analyzed the strain-time curves either by identifying the stress value marking the onset of linear growth, or by measuring the ratio between the recovered strain γ_{OFF} and the maximum accumulated strain γ_{ON} (see Fig. 4a). The latter quantity is plotted in Fig. 4c as a function of the applied stress. Two regimes are observed: at low applied stress most of the strain is recovered, while the ratio progressively departs from unity and drops for increasing stresses. We alternatively identify σ_y as the crossover between these two regimes[35] (dashed lines in Fig. 4c), which leads to a similar, slightly lower estimate as compared to the previous criterion (linear growth in strain-time curves), but with remarkably similar behaviour to macroscopic measurements. Indeed, it is known that σ_y estimates significantly depend on the adopted rheological tests[35]. We plot the determined σ_y values as a function of

View Article Online
DOI: 10.1039/D0SM02168G

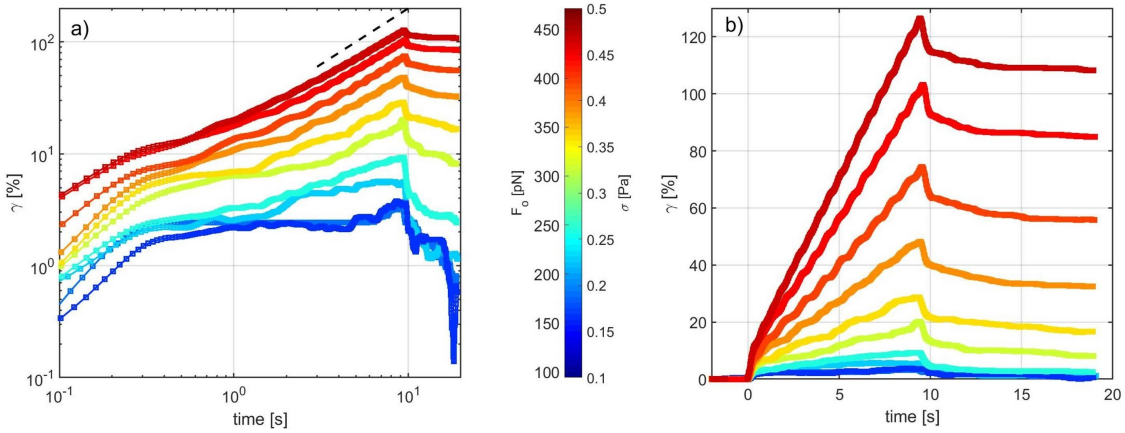

Fig. 3 Results of the creep and recovery measurements performed on an Aqua sample at c = 0.375% using the microrheology setup. The measurements were performed by imposing different force - or stress - values, as indicated by the color bars. The resulting strain-time curves are shown in a) logarithmic and b) linear scale.

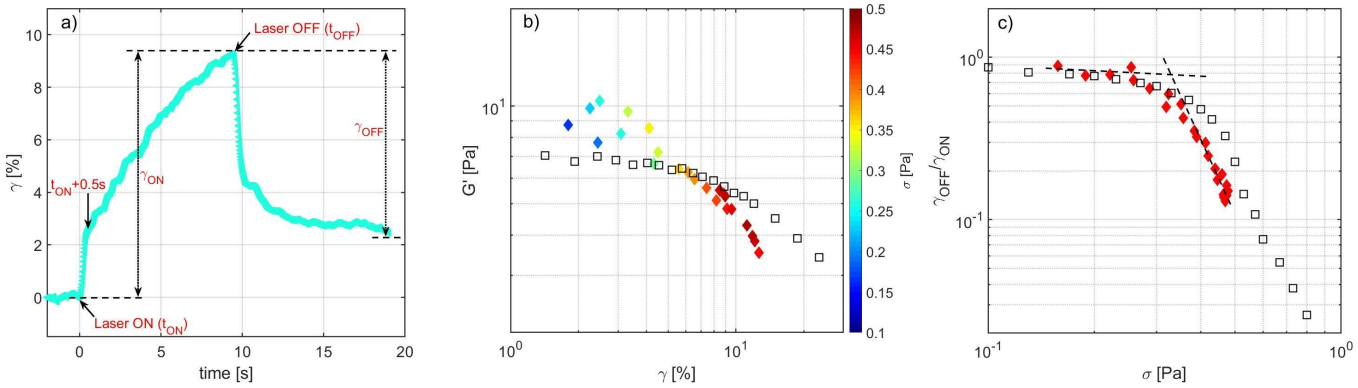

Fig. 4 Analysis of the creep and recovery microrheology experiments performed on an Aqua sample at c = 0.375% and comparison with the results obtained from macroscopic measurements. a) Example of a single curve obtained from microrheology experiments at a stress value $\sigma = 0.26$ Pa in which the different parameters used in the analysis are reported. The laser radiation is switched ON and OFF at times t_{ON} and t_{OFF}, respectively, while the short-time elastic component of the material is estimated at a time $t_{ON} + 0.5s$. The parameters γ_{ON} and γ_{OFF} indicate the maximum accumulated strain and the recovered strain during the experiments, respectively; b) Comparison of the short-time elastic component G' resulting from microrheology (colored diamonds) and macrorheology (empty squares) experiments as a function of strain. The color bar is used to indicate the stress values employed in microrheology tests; c) Comparison of the ratio γ_{OFF}/γ_{ON} resulting from microrhology (red diamonds) and macrorheology (empty squares) experiments as a function of the applied stress.

Aqua concentration in Fig. 5. We find a good agreement, with microscopic values slightly below the macroscopic ones but similar dependence on concentration. This correspondence is not obvious, as a number of factors, including probe size, surface chemistry and sample heterogeneity, can critically affect the agreement between macro- and microrheology results and break down the continuum response[22,32,36].

3.2.1 Fluid regime

When the applied stresses are high enough to induce fluidization of the material, the resulting motion of the microbead is linear in time. We convert its speed v into a strain rate ($\dot{\gamma} = v/2R$), an average value of the strain rates around the probe[22], and compare it to the stress-strain rate relationship from the corresponding macroscopic creep measurements in Fig. 6a (blue up triangles and black down triangles, respectively). Despite the simplifications, the values are similar and display the same trend: at low shear rates the stress tends to finite values, corresponding to a divergence of the effective viscosity. The results are also in agreement with a steady shear experiment (empty green squares) and are well described by a Herschel-Bulkley model $\sigma = \sigma_y + K\dot{\gamma}^n$, which provides alternative access to yield stress estimation. In Fig. 5, in the calculation of the average yield stress values from macrorheology measurements we also included the σ_y estimates from Herschel-Bulkley fits of the bulk steady shear experiments.

3.2.2 Microscopic signatures

Despite the observed qualitative and quantitative agreement with bulk measurements, the microscopic trajectories show distinctive features which reflect the finite size of the sample building blocks, as visible in Fig. 3. At low applied stresses (blue to green lines), the bead displays an intermittent motion during the creep stage, with small jumps intercalated by rest intervals. At higher stresses (orange to red lines), the motion of the bead becomes progres-

View Article Online
DOI: 10.1039/D0SM02168G

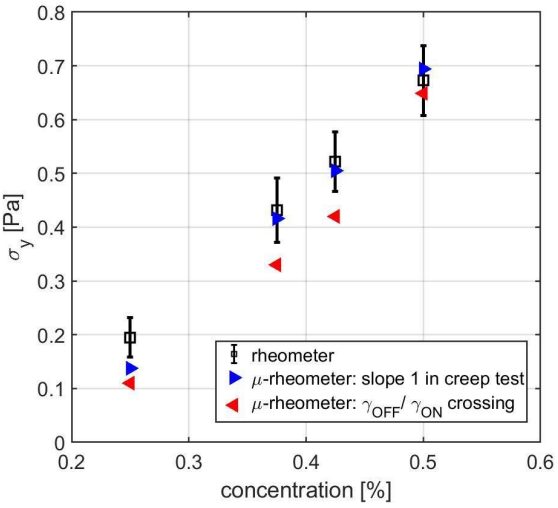

Fig. 5 Yield stress values σ_y as a function of Aqua concentration. The σ_y values from microrheological experiments were determined according to two different approaches: identification of the stress value marking the onset of linear growth in strain-time curves (blue right triangles) and crossing between the low- and high-stress regimes identified by the γ_{OFF}/γ_{ON} ratio (red left triangles). In addition to the two above mentioned approaches, for the calculation of the average σ_y values for macrorheology experiments (black empty squares), we also included σ_y estimates from Herschel-Bulkley fits of the bulk steady shear experiments.

sively more regular, but the trajectories are nonetheless composed of a series of bounces. To quantitatively characterize the different features of microbead motion, we performed temporal and spatial Fourier analysis of the bead velocity (Fig. 6b and c). At low stresses, there is a wide distribution of temporal frequencies, reflecting the intermittent nature of creep motion; instead, at higher stresses, one single temporal frequency dominates for each stress value, indicating a periodic motion of the microbead advancing within the packed microgels, with regular steps of acceleration and slowing down. Such frequency increases with increasing stress (Fig. 6b). However, at all stresses one single spatial frequency emerges, corresponding to steps of about 700 nm, much smaller than the microbead diameter (10 μm) and corresponding to ~ 1.5 times the swollen microgel diameter, as estimated by dynamic light scattering on dilute samples ($r_H = 250nm$). By indicating with f_{temp} and f_{spat} the dominant temporal and spatial frequencies, respectively, we observe that the strain rates, calculated as $\dot{\gamma} = f_{temp}/(2R \cdot f_{spat})$, coincide with the previous estimate based on the direct assessment of microbead velocity (red crosses in Fig. 6a).

Given that the microgels are significantly smaller than the microbead, a quasi-continuum response can be expected[22]. However, since the bulk strain curves show neither the intermittent nor the periodic behaviour, this microscopic feature likely results from local rearrangements of a few particles around the probe, triggered by its push, as evidenced by the 700 nm jumps. The effect of a force upon a non-Brownian particle in a soft glass (made of the same elastic particles) has been investigated in molecular dynamics simulations[37]. A transition between caged and translating probe was found for increasing forces, together with quantitative correspondence with macroscopically measured viscosity. Particles were found to accumulate in the direction of motion and deplete in the rear. A similar anisotropic distribution, with a denser and a sparser region in front and behind the probe particle, respectively, was experimentally found with active laser tweezer microrheology in a dense colloidal suspension[20], with probe-to-sample size ratio between 6 and 20. Also in our case, microgels are likely compressed in front of the forced probe and depleted behind it, which may explain the approximately constant value of immediate, elastic recoil when the high stresses are removed (Fig. 3b).

3.2.3 Size of the yielded region

To image the response of the portion of material surrounding the probe during stress application and removal[21,38,39], we seeded the microgel samples with small, passive tracers.

In Fig. 7 we display representative snapshots for the initial condition before the optical shooting (a), for the maximum deformation (b) and for the final state after recovery (c), upon application of a high stress which induces permanent displacement of the microbead. As highlighted by the arrows in panels b and c (drawn from image differences b-a and c-a, respectively, see Supplementary Fig. S3), while the tracers far from the microbead only undergo an elastic deformation, recovered upon stress removal, the tracers closer to the microbead are permanently displaced, as a result of plastic deformation, or fluidization, of the nearby region. Although we lack the temporal and spatial resolution to fully describe the evolution of the strain field, by averaging several of such experiments we can reconstruct the typical size of the fluidized region for each applied stress (see Supplementary Fig. S3). In Fig. 7d, we plot, in units of the microbead radius R, the average distance of the farthest tracer permanently displaced after recovery at each applied stress. While for low stresses only elastically deformed material can be detected around the microbead, at yield stress we observe the sharp onset of a fluidized region of about $2R$, whose size slightly grows for increasing stress. Such values seem consistent with the prefactor in the denominator of Eq. 2, which we adopted to convert the optical force into a stress by extension of Stokes drag. Indeed, this is equivalent to assuming that the effective cross-section is $\pi R_{eff}^2 = 6\pi R^2$ or $R_{eff} \approx 2.45R$. Furthermore, the extent of the affected region is also consistent to Y values in Eq. 1 between 0.14 and 0.2, the range of previous theoretical and experimental estimates for mm-sized spheres in similar soft, packed systems[7,10–12,37]. The detailed value, as well as stress decay within the sample, may depend on the shear thinning properties of the specific systems[37] and on their microstructure. For example, larger affected regions were found in networked materials like microfibrous cellulose[7] or Laponite clay[18], but a smaller region was reported for an optically rotated microdisk in gelatin[40]. Overall, stress-induced yielding appears as a spatially heterogeneous transition, that gradually propagates across the material, while some residual elasticity persists also in the flow regime[41]. A more detailed reconstruction of the strain field around the microbead could help to separate the shear and compression components of material's response[18] and to systematically address the correspondence between macroscopic and mi-

View Article Online
DOI: 10.1039/D0SM02168G

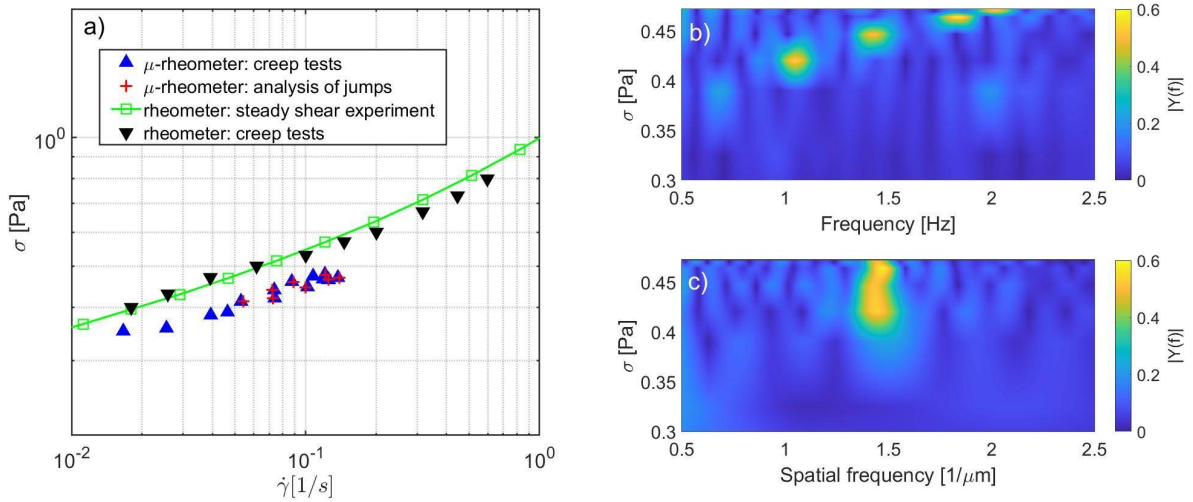

Fig. 6 a) Comparison of stress-strain rate relationship obtained from macro- and microrheology experiments performed on an Aqua sample at c = 0.375%; b) Temporal and c) spatial Fourier transform of the microbead velocity derived from micro-creep trajectories, for different values of the applied stress. At low stresses, no dominant frequency can be identified, reflecting the intermittent nature of creep motion, while, at higher stresses, one single frequency dominates for each stress value. Such frequency increases with increasing stress for the temporal Fourier spectrum (panel b), whereas one single spatial frequency emerges in the spatial Fourier spectrum (panel c).

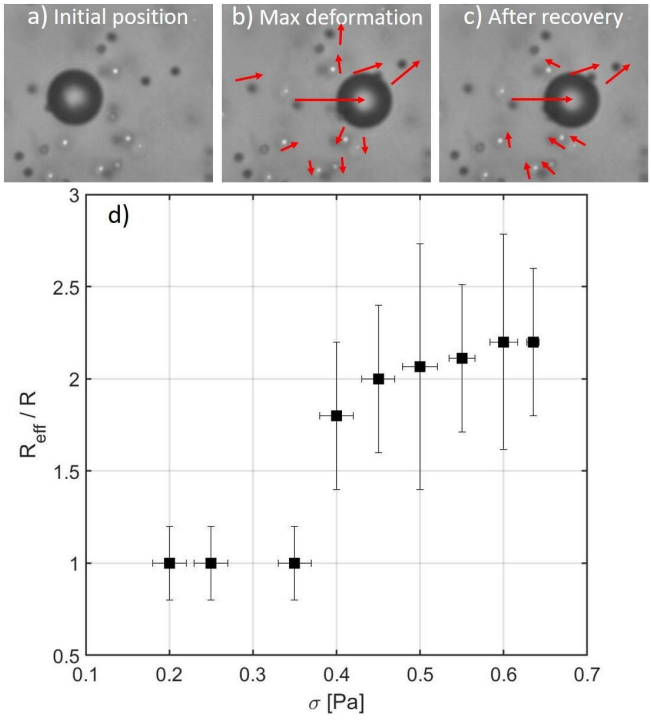

Fig. 7 Results from the imaging experiments performed on an Aqua sample at c = 0.375%. Snapshots of the a) initial state before the optical shooting, b) maximum deformation state, c) final state at the end of the recovery phase, obtained from a video-imaging experiment performed at $\sigma = 0.45$Pa. The red arrows highlight the displacement of the tracers. d) Effective size of the fluidized region R_{eff}, in units of the bead radius R, as a function of the applied stress σ.

croscopic measurements while changing sample and microbead properties. Further information may also come from embedded probes of local strain at the nanoscale[42].

4 Conclusions

We have reported yield stress measurements in packed microgels through an optofluidic active microrheology setup based on optical scattering forces impinging on a microbead. The combination of a powerful IR laser, waveguides written in glass and microbead with high refractive index provides forces exceeding 1 nN and stresses in the Pa range with a 5 μm radius particle. We have performed creep and recovery tests at the microscale, finding qualitative and quantitative agreement with bulk rheology measurements for the different low and high stress regimes and at short and long time scales, from elastic response to creep and fluidization. However, a rich behaviour emerges in microscale experiments, with intermittent motion at low stresses and periodic, small jumps at higher stresses, which reflect rearrangements within the microgel suspension. The extent of the plastically deformed portion of material around the microbead, as extracted from dispersed tracers, is in agreement with the adopted definition of stress and with previous experiments on the stability criteria for spheres in yield stress materials. The device and approach here reported allow determination of yield stress in microliter volumes and are therefore well suited for precious or poorly available samples.

Author contributions

G.Z. designed and coordinated the research. F.B., P.P. and R.O. designed and fabricated the optofluidic chip. V.V., G.N., A.C., M.P., G.Z. performed the microrheology experiments. M.A.O. and G.Z. performed the bulk rheology experiments. V.V., G.N., A.C., M.P., I.C., P.M., T.B. and G.Z. analyzed the results. All the authors discussed the results. G.Z. and V.V. drafted the manuscript and all the authors edited it.

View Article Online
DOI: 10.1039/D0SM02168G

Conflicts of interest

There are no conflicts to declare.

Acknowledgements

We thank Giovanni Scandella (Biochim s.r.l.) for the kind gift of Aqua sample and Federica Cremaschi for preliminary measurements. We also acknowledge inspiring discussions with Marco Caggioni and Veronique Trappe and thank Paolo Edera for critical reading of the manuscript. This work was supported by the University of Milano (Piano sviluppo Unimi 2018 Biometra).

Notes and references

1 R. Chhabra, *Bubbles, Drops and Particles in Non-Newtonian Fluids*, CRC Press, 2nd edn, 2006.
2 D. Bonn, M. M. Denn, L. Berthier, T. Divoux and S. Manneville, *Reviews of Modern Physics*, 2017, **89**, 035005.
3 N. J. Balmforth, I. A. Frigaard and G. Ovarlez, *Annual Review of Fluid Mechanics*, 2014, **46**, 121–146.
4 P. Coussot, *Rheologica Acta*, 2018, **57**, 1–14.
5 A. Z. Nelson and R. H. Ewoldt, *Soft Matter*, 2017, **13**, 7578–7594.
6 G. Zanchetta, S. Mirzaagha, V. Guida, F. Zonfrilli, M. Caggioni, N. Grizzuti, R. Pasquino and V. Trappe, *Colloid and Polymer Science*, 2018, **296**, 1379–1385.
7 H. Emady, M. Caggioni and P. Spicer, *Journal of Rheology*, 2013, **57**, 1761–1772.
8 S. Mirzaagha, R. Pasquino, E. Iuliano, G. D'Avino, F. Zonfrilli, V. Guida and N. Grizzuti, *Physics of Fluids*, 2017, **29**, 093101.
9 G. Astarita, *Journal of Rheology*, 1990, **34**, 275–277.
10 A. N. Beris, J. A. Tsamopoulos, R. C. Armstrong and R. A. Brown, *Journal of Fluid Mechanics*, 1985, **158**, 219–244.
11 D. D. Atapattu, R. P. Chhabra and P. H. Uhlherr, *Journal of Non-Newtonian Fluid Mechanics*, 1995, **59**, 245–265.
12 H. Tabuteau, P. Coussot and J. R. de Bruyn, *Journal of Rheology*, 2007, **51**, 125–137.
13 Y. Holenberg, O. M. Lavrenteva, U. Shavit and A. Nir, *Physical Review E - Statistical, Nonlinear, and Soft Matter Physics*, 2012, **86**, 066301.
14 A. M. Putz, T. I. Burghelea, I. A. Frigaard and D. M. Martinez, *Physics of Fluids*, 2008, **20**, 033102.
15 T. A. Waigh, *Reports on Progress in Physics*, 2016, **79**, 074601.
16 L. G. Wilson and W. C. Poon, *Physical Chemistry Chemical Physics*, 2011, **13**, 10617–10630.
17 J. Lin and M. T. Valentine, *Review of Scientific Instruments*, 2012, **83**, 053905.
18 J. P. Rich, J. Lammerding, G. H. McKinley and P. S. Doyle, *Soft Matter*, 2011, **7**, 9933–9943.
19 A. Ashkin, J. M. Dziedzic, J. E. Bjorkholm and S. Chu, *Optics Letters*, 1986, **11**, 288.
20 A. Meyer, A. Marshall, B. G. Bush and E. M. Furst, *Journal of Rheology*, 2006, **50**, 77–92.
21 R. M. Robertson-Anderson, *ACS Macro Letters*, 2018, **7**, 968–975.
22 T. M. Squires and T. G. Mason, *Annual Review of Fluid Mechanics*, 2010, **42**, 413–438.
23 A. Ashkin, *Physical Review Letters*, 1970, **24**, 156–159.
24 R. M. Vazquez, R. Osellame, D. Nolli, C. Dongre, H. Van Den Vlekkert, R. Ramponi, M. Pollnau and G. Cerullo, *Lab on a Chip*, 2009, **9**, 91–96.
25 F. Bragheri, L. Ferrara, N. Bellini, K. C. Vishnubhatla, P. Minzioni, R. Ramponi, R. Osellame and I. Cristiani, *Journal of Biophotonics*, 2010, **3**, 234–243.
26 T. Yang, G. Nava, V. Vitali, F. Bragheri, R. Osellame, T. Bellini, I. Cristiani and P. Minzioni, *Micromachines*, 2017, **8**, 65.
27 V. Vitali, G. Nava, G. Zanchetta, F. Bragheri, A. Crespi, R. Osellame, T. Bellini, I. Cristiani and P. Minzioni, *Scientific Reports*, 2020, **10**, 1–11.
28 G. Nava, T. Yang, V. Vitali, P. Minzioni, I. Cristiani, F. Bragheri, R. Osellame, L. Bethge, S. Klussmann, E. M. Paraboschi, R. Asselta and T. Bellini, *Soft Matter*, 2018, **14**, 3288–3295.
29 G. P. Roberts and H. A. Barnes, *Rheologica Acta*, 2001, **40**, 499–503.
30 T. Yang, Y. Chen and P. Minzioni, *Journal of Micromechanics and Microengineering*, 2017, **27**, 123001.
31 L. Ferrara, E. Baldini, P. Minzioni, F. Bragheri, C. Liberale, E. D. Fabrizio and I. Cristiani, *Journal of Optics*, 2011, **13**, 75712–75719.
32 M. T. Valentine, Z. E. Perlman, M. L. Gardel, J. H. Shin, P. Matsudaira, T. J. Mitchison and D. A. Weitz, *Biophysical Journal*, 2004, **86**, 4004–4014.
33 R. M. Evans, M. Tassieri, D. Auhl and T. A. Waigh, *Physical Review E - Statistical, Nonlinear, and Soft Matter Physics*, 2009, **80**, 012501.
34 R. Rivas-Barbosa, M. A. Escobedo-Sánchez, M. Tassieri and M. Laurati, *Physical chemistry chemical physics : PCCP*, 2020, **22**, 3839–3848.
35 M. Dinkgreve, J. Paredes, M. M. Denn and D. Bonn, *Journal of Non-Newtonian Fluid Mechanics*, 2016, **238**, 233–241.
36 R. Holyst, A. Bielejewska, J. Szymański, A. Wilk, A. Patkowski, J. Gapiński, A. Zywociński, T. Kalwarczyk, E. Kalwarczyk, M. Tabaka, N. Zibacz and S. A. Wieczorek, *Physical Chemistry Chemical Physics*, 2009, **11**, 9025–9032.
37 L. Mohan, M. Cloitre and R. T. Bonnecaze, *Journal of Rheology*, 2014, **58**, 1465–1482.
38 M. H. Lee and E. M. Furst, *Physical Review E - Statistical, Nonlinear, and Soft Matter Physics*, 2008, **77**, 041408.
39 D. Anderson, D. Schaar, H. G. Hentschel, J. Hay, P. Habdas and E. R. Weeks, *Journal of Chemical Physics*, 2013, **138**, 12A520.
40 J. N. Wilking and T. G. Mason, *Physical Review E - Statistical, Nonlinear, and Soft Matter Physics*, 2008, **77**, 055101.
41 G. J. Donley, P. K. Singh, A. Shetty and S. A. Rogers, *Proceedings of the National Academy of Sciences*, 2020, 202003869.
42 G. Zanchetta, *Current Opinion in Colloid and Interface Science*, 2019, **40**, 1–13.